14C.2 ASPECTS OF CHAOTIC MIXING IN THE HURRICANE INNER-CORE

Eric A. Hendricks* and Wayne H. Schubert
Colorado State University, Fort Collins, Colorado

1. INTRODUCTION

Mixing is due to the combined effect of differential advection and turbulent (or inevitably, molecular) diffusion. Differential advection (stirring) stretches and deforms material lines from which diffusion accomplishes true irreversible mixing. The interplay between advection and diffusion in mixing makes it difficult to quantify. Even in rather simple unsteady nonturbulent flows, the phenomenon known as chaotic advection, where particle trajectories are not integrable, has been shown to exist (Aref 1982, Ottino 1989). Recent work has proposed the use of an area (Nakamura 1996; Winters and D'Asaro 1996, Shuckburgh and Haynes 2003) hybrid Eulerian-Lagrangian coordinate system that separates the reversible effects of advection (absorbed into the coordinate) with the irreversible effects of diffusion. When transforming the advection-diffusion equation into the area coordinate, an effective diffusion (diffusion only) equation is obtained with a diagnostic coefficient of the equivalent length (Nakamura 1996) of a tracer contour. As this equivalent length becomes large there is more interface for diffusion to act and the "effective diffusivity" is larger. The effective diffusivity thus encompasses aspects of both differential advection and diffusion in mixing. Shuckburgh and Haynes (2003) demonstrated that effective diffusivity is a well-defined flow diagnostic for a chaotic time-periodic flow.

In recent work the effective diffusivity diagnostic has been used to quanitify transport and mixing properties in the upper tropophere and stratosphere (see Haynes and Shuckburgh 2000a,b, Allen and Nakamura 2001, Scott et al. 2003 and references therein). That work complements the previous use of Lyapunov exponents (e.g., Lapeyre 2002) in large-scale transport and mixing (e.g., Pierrhumbert and Yang 1993, Ngan and Shepherd 1999a,b). In the present work, we apply the effective diffusivity diagnostic to aperiodic chaotic advective hurricane-like flows. In three dimensions, transport and mixing can be quite complicated due to interactions of multiscale three dimensional eddies, from the Kolmogorov inertial range to mesovortices that have been observed at scales of 10-50 km. In order to make this problem initially more tractable, we focus our study on two-dimensional hurricane-like vortices in a nondivergent barotropic model framework. As an initial example, a numerical solution to the nondivergent barotropic vorticity equation and the advection-diffusion equation is obtained for the evolution of an elliptical vorticity field, and the effective diffusivity diagnostic is used to quantify mixing properties during its evolution. The transport and mixing properties of other barotropic hurricane-like vortices will be shown in the presentation.

2. DYNAMICAL MODEL AND PASSIVE TRACER EQUATION

The dynamical model used here considers two-dimensional, nondivergent motions on a plane. The governing vorticity equation is

$$\frac{\partial \zeta}{\partial t} + \mathbf{u} \cdot \nabla \zeta = \nu \nabla^2 \zeta, \qquad (1)$$

where $\mathbf{u} = \mathbf{k} \times \nabla \psi$ is the horizontal, nondivergent velocity, $\zeta = \nabla^2 \psi$ is the relative vorticity, and ν is the constant viscosity. The solutions presented here were obtained with a double Fourier pseudospectral code having 768×768 equally spaced points on a doubly periodic, 600 km $\times$ 600 km domain. Since the code was run with a dealiased calculation of the nonlinear term in (1), there were 256×256 resolved Fourier modes. The wavelength of the highest Fourier mode is 2.3 km. A fourth-order Runge-Kutta scheme was used for time differencing, with a 3.5 s time step. The value of viscosity was chosen to be $\nu = 50$ m^2 s^{-1}, so the characteristic damping time for modes having total wavenumber equal to 256 is 2.4 hours, while the damping time for modes having total wavenumber equal to 170 is 5.5 hours.

As a way to understand the transport and mixing properties of an evolving flow described by (1), it is useful to also calculate the evolution of a passive tracer subject to diffusion and to advection by the

---
*Corresponding author address: Eric Hendricks, Department of Atmospheric Science, Colorado State University, Fort Collins, CO 80523-1375; e-mail: eric@atmos.colostate.edu

nondivergent velocity $\mathbf{u}$. The advection-diffusion equation for this passive tracer is

$$\frac{\partial c}{\partial t} + \mathbf{u} \cdot \nabla c = \nabla \cdot (\kappa \nabla c), \qquad (2)$$

where $c(x, y, t)$ is the concentration of the passive tracer and κ is the constant diffusivity. The numerical methods used to solve (2) are identical to those used to solve (1). However, the results to be presented here have quite different initial conditions on ζ and c. The passive tracer c is always initialized as an axisymmetric and monotonic function. We have chosen both linear and Gaussian functions with maxima at the vortex center. In contrast, the initial vorticity is not necessarily montonic with radius (e.g., it may have the form of a barotropically unstable vorticity ring) and is not necessarily axisymmetric.

3. AREA COORDINATE TRANSFORMATION AND EFFECTIVE DIFFUSIVITY

To aid in the derivation a diagram of the area coordinate is shown in Fig. 1. Consider the transform from Cartesian (x, y) coordinates to tracer (C, s) coordinates, where C is a particular contour of the $c(x, y, t)$ field and s is the position along that contour. Let dC be the differential element of C and ds be the differential element of s. Let $A(C, t)$ denote the area of the region in which the tracer concentration satisfies $c(x, y, t) \geq C$, i.e.,

$$A(C, t) = \iint_{c \geq C} dx\, dy. \qquad (3)$$

Let $\gamma(C, t)$ denote the boundary of this region. Note that $A(C, t)$ is a monotonically decreasing function of C and that $A(C_{max}, t) = 0$. Now define $\mathbf{u}^C$ as the velocity of the contour C, so that

$$\frac{\partial c}{\partial t} + \mathbf{u}^C \cdot \nabla c = 0. \qquad (4)$$

Noting that $\nabla c / |\nabla c|$ is the unit vector normal to the contour, we can use (3) and (4) to write

$$\frac{\partial A(C, t)}{\partial t} = \frac{\partial}{\partial t} \iint_{c \geq C} dx\, dy$$

$$= -\int_{\gamma(C,t)} \mathbf{u}^C \cdot \frac{\nabla c}{|\nabla c|} ds \qquad (5)$$

$$= \int_{\gamma(C,t)} \frac{\partial c}{\partial t} \frac{ds}{|\nabla c|},$$
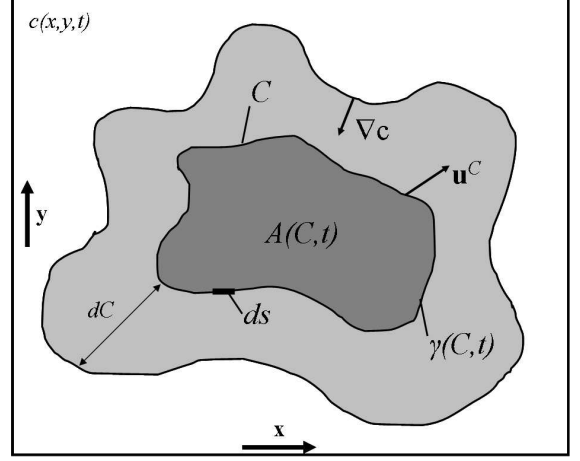

Figure 1: Diagram of the area coordinate. Two hypothetical contours C of the tracer field $c(x, y, t)$ are shown with corresponding area above the contours $A(C, t)$. The other parameters used in the derivation are illustrated as well.

where ds is an increment of distance along the tracer contour. Using (2) in the last equality of (5) we obtain

$$\frac{\partial A(C, t)}{\partial t} = \int_{\gamma(C,t)} \nabla \cdot (\kappa \nabla c) \frac{ds}{|\nabla c|} - \int_{\gamma(C,t)} \mathbf{u} \cdot \nabla c \frac{ds}{|\nabla c|}. \qquad (6)$$

We now note that (since $dx\, dy = ds\, dC'/|\nabla c|$)

$$\frac{\partial}{\partial C} \iint_{c \geq C} (\ ) \, dx\, dy = \frac{\partial}{\partial C} \iint_{c \geq C} (\ ) \frac{ds\, dC'}{|\nabla c|}$$

$$= -\int_{\gamma(C,t)} (\ ) \frac{ds}{|\nabla c|}. \qquad (7)$$

Using (7) in (6) while noting that $\mathbf{u} \cdot \nabla c = \nabla \cdot (c\mathbf{u})$ because $\mathbf{u}$ is nondivergent, we obtain

$$\frac{\partial A(C, t)}{\partial t} = -\frac{\partial}{\partial C} \iint_{c \geq C} \nabla \cdot (\kappa \nabla c) \frac{ds\, dC'}{|\nabla c|}$$

$$+ \frac{\partial}{\partial C} \iint_{c \geq C} \nabla \cdot (c\mathbf{u}) \frac{ds\, dC'}{|\nabla c|}$$

$$= -\frac{\partial}{\partial C} \int_{\gamma(C,t)} \kappa |\nabla c| ds$$

$$+ \frac{\partial}{\partial C} \int_{\gamma(C,t)} c\mathbf{u} \cdot \frac{\nabla c}{|\nabla c|} ds. \qquad (8)$$

The third and fourth lines of (8) are obtained using the divergence theorem. The fourth line of (8) vanishes because the factor c in the integrand can come

outside the integral, leaving $\int_{\gamma(C,t)} \mathbf{u} \cdot (\nabla c/|\nabla c|) ds$, which vanishes because $\mathbf{u}$ is nondivergent.

Since $A(C,t)$ is a monotonic function of C, there exists a unique inverse function $C(A,t)$. We now transform (8) from a predictive equation for $A(C,t)$ to a predictive equation for $C(A,t)$. This transformation is aided by

$$\frac{\partial A(C,t)}{\partial t}\frac{\partial C(A,t)}{\partial A} = -\frac{\partial C(A,t)}{\partial t}, \qquad (9)$$

which, when used in (8), yields

$$\frac{\partial C(A,t)}{\partial t} = \frac{\partial C(A,t)}{\partial A}\frac{\partial}{\partial C}\int_{\gamma(C,t)}\kappa|\nabla c|\,ds$$
$$= \frac{\partial}{\partial A}\int_{\gamma(C,t)}\kappa|\nabla c|\,ds. \qquad (10)$$

Because of (7), the integral $\int_{\gamma(C,t)}\kappa|\nabla c|\,ds$ on the right hand side of (10) can be replaced by $(\partial/\partial C)\iint_{c\geq C}\kappa|\nabla c|^2\,dx\,dy$. Then, (10) can be written in the form

$$\frac{\partial C(A,t)}{\partial t} = \frac{\partial}{\partial A}\left(K_{eff}(A,t)\frac{\partial C(A,t)}{\partial A}\right), \qquad (11)$$

where

$$K_{eff}(A,t) = \left(\frac{\partial C}{\partial A}\right)^{-2}\frac{\partial}{\partial A}\iint_{c\geq C}\kappa|\nabla c|^2 dx\,dy. \qquad (12)$$

To summarize, we have used the area coordinate to transform the advection-diffusion equation (2) into the diffusion-only equation (11), in the process yielding the effective diffusivity $K_{eff}(A,t)$. Since $K_{eff}(A,t)$ can be computed from (12), it can serve as a useful diagnostic tool to help understand the interplay of advection and diffusion in (2). However, note that, because of the use of A as an independent variable, the effective diffusivity $K_{eff}(A,t)$ has the rather awkward units $m^4\,s^{-1}$. This is easily corrected by mapping the area coordinate into the equivalent radius coordinate r_e, which is defined by $\pi r_e^2 = A$. Thus, transforming (11) to the equivalent radius using $2\pi r_e(\partial/\partial A) = (\partial/\partial r_e)$, we obtain

$$\frac{\partial C(r_e,t)}{\partial t} = \frac{\partial}{r_e\partial r_e}\left(r_e\kappa_{eff}(r_e,t)\frac{\partial C(r_e,t)}{\partial r_e}\right) \qquad (13)$$

where

$$\kappa_{eff}(r_e,t) = \frac{K_{eff}(A,t)}{4\pi A}. \qquad (14)$$

Note that, with of the use of r_e as an independent variable, the effective diffusivity $\kappa_{eff}(r_e,t)$ has the units $m^2\,s^{-1}$.

The effective diffusivity diagnostic $\kappa_{eff}(r_e,t)$ can be calculated at a given time t from the output $c(x,y,t)$ of the numerical solution of (2). The calculation of $K_{eff}(A,t)$ involves the following discrete approximation of the right hand side of (12). First, the desired number of area coordinate points is chosen ($n_A = 200$ for the results shown here). The tracer contour interval (ΔC) is set using $\Delta C = [max(c) - min(c)]/n_A$. Next, $|\nabla c|^2$ is calculated at each model grid point. Then, a discrete approximation of the function $A(C,t)$ is determined by adding up the area within each chosen C contour, i.e., by using a discrete approximation to (3). The discrete approximation to $A(C,t)$ is then converted to a discrete approximation of its inverse, $C(A,t)$. The denominator of the effective diffusivity diagnostic, $(dC/dA)^2$, is calculated by taking second order accurate finite differences of $C(A,t)$. The numerator of the right hand side of (12) is then calculated in the same manner. which completes the calculation of the effective diffusivity $K_{eff}(A,t)$. The equivalent radius effective diffusivity diagnostic $\kappa_{eff}(r_e,t)$ is then easily computed using (14). As will be shown, plots of the diagnostic reveal the locations and magnitude of partial barrier and mixing regions in the vortex.

In the next section, two-dimensional plots of effective diffusivity will be shown. This can be done because effective diffusivity is constant along a tracer contour, and tracer contours meander in (x, y) space. From another point of view, $\kappa_{eff}(r_e,t)$ can be mapped to $\kappa_{eff}(x,y,t)$ because each horizontal grid point is associated with an equivalent radius.

4. PSEUDOSPECTRAL MODEL EXPERIMENT AND RESULTS

The initial elliptical vorticity field is contructed in a manner similar to Guinn (1992). In polar coordinates, the initial vorticity field is specified by

$$\zeta(r,\phi,0) = \zeta_0\begin{cases}1 & 0 \leq r \leq r_i\alpha(\phi) \\ 1 - f_\lambda(r') & r_i\alpha(\phi) \leq r \leq r_0\alpha(\phi), \\ 0 & r_0\alpha(\phi) \leq r\end{cases} \qquad (15)$$

where $\alpha(\phi)$ is an ellipticity augmentation factor described in the next paragraph. Here, ζ_0 is the maximum vorticity at the center, $f_\lambda(r') = \exp[-(\lambda/r')\exp(1/(r'-1))]$ is a monotonic shape function with transition steepness parameter λ, $r' =$
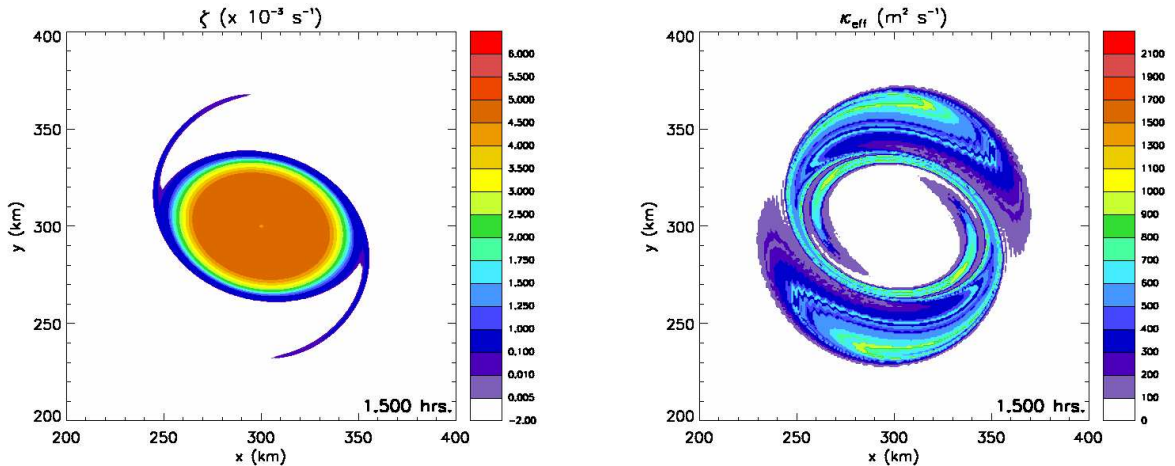
Figure 2: Side-by-side panels of relative vorticity and effective diffusivity for the evolution of the elliptical vorticity field at $t = 1.5$ h.

$(r - r_i\alpha(\phi))/(r_0\alpha(\phi) - r_i\alpha(\phi))$ is a nondimensional radius proportional to $r = (x^2 + y^2)^{1/2}$, and r_i and r_0 are the radii where the vorticity begins to decrease and where it vanishes, respectively. For the special case of $\alpha(\phi) = 1$ the field is axisymmetric.

This field may then be deformed to an ellipse by specifying an eccentricity $\epsilon = (1 - (b^2/a^2))^{1/2}$, where a is the semi-major axis and b is the semi-minor axis of the ellipse $(x/a)^2 + (y/b)^2 = 1$. Using the eccentricity and the angle ϕ, an augmentation factor $\alpha(\phi) = ((1 - \epsilon^2)/(1 - \epsilon^2 \cos^2(\phi)))^{1/2}$ may be defined, and when used in (15) the field is changed to elliptical for $0 < \epsilon < 1$. For the experiment conducted, $\lambda = 2.0$, the eccentricity $\epsilon = 0.70$ corresponding to the semi-major axis approximately twice as large as the semi-minor axis, and the radii r_i and r_0 were set to 30 km and 60 km, respectively.

Side-by-side plots of vorticity and effective diffusivity at $t = 1.5$ h during the evolution of the elliptical vorticity field are shown in Fig. 2. At this time, two filaments of high vorticity (breaking vortex Rossby waves) are clearly visible. Associated with these filaments are regions of large effective diffusivity. The effective diffusivity peaks just upwind of the filaments and extends further upwind. The main vortex acts as a transport barrier during the filamentation. In terms of an arbitrary passive tracer, these results indicate that the tracer will tend to be well-mixed horizontally in the wave breaking "surf zone" (cf. Guinn and Schubert 1993), and tracers initially in the vortex core will be trapped there forever. During its evolution, continued wave breaking episodes occur as the ellipse tries to axisymmetrize. Axisymmetrization is not complete here within $t \leq 48$ h however and the surf zone is

a robust feature throughout the entire simulation. The ability of an elliptical vorticity field to axisymmetrize (Melander et al. 1987) via inviscid dynamics was shown to be determined by the sharpness of its edge (Dritschel 1998). If the vortex is more Rankine-like (i.e., possessing a sharp edge), it will tend to rotate and not generate filaments. If, on the other hand, the transition is more Gaussian, there will be a tendency to generate filaments and axisymmetrize. Based on the above results, we hypothesize that the latter vortex would exhibit a stronger and larger surf zone.

Although it occurs on much smaller time and length scales, there is an analogy between this surf zone in tropical cyclones and the planetary Rossby wave breaking surf zone associated with the wintertime stratospheric polar vortices (McIntyre and Palmer 1983, 1984, 1985, McIntyre 1989; Juckes and McIntyre 1987, Bowman 1993, Waugh et al. 1994). Planetary waves excited in the troposphere may propagate vertically and cause wave breaking to occur on the edge of the stratospheric polar vortex, from which chemical constituents such as ozone can be mixed into the midlatitudes. The wintertime stratospheric polar vortices display similar processes to our experiment, namely the core vortex is a transport barrier and the surf zone is a chaotic mixing region. The existence of the main vortex barrier was thought to be due to the strong PV gradient, a restoring mechanism for perturbations imposed upon it. Rossby wave breaking has also been examined in more idealized frameworks (Polvani and Plumb 1992, Bowman 1995, Koh and Plumb 2000).

In tropical cyclones, the deformation of an initially circular vortex core to an ellipse may hap-

pen due to external (e.g., vertical shear) or internal (e.g., PV generation by asymmetric moist convection) processes. Low wavenumber deformations to the hurricane inner-core are often observed (Reasor et al. 2000, Corbosiero et al. 2006). The relaxation to axisymmetry may produce wave breaking episodes, and, as we have shown here, moderate mixing regions in the associated surf zone.

5. CONCLUSION

The derivation of effective diffusivity was reviewed, and an equivalent radius coordinate was defined to aid in determining the location of partial barrier and mixing regions in a hurricane-like vortex. The diagnostic was applied to a nondivergent barotropic model simulation of an elliptical vorticity field. The diagnostic was able to capture both the central vortex partial barrier and the PV wave breaking surf zone mixing regions. Complementing Lagrangian trajectory methods (e.g., Cram et al. 2007), we feel effective diffusivity is a useful tool to aid in understanding transport and mixing properties of hurricanes.

6. REFERENCES

Allen DR, and Nakamura N. 2001. A seasonal climatology of effective diffusivity in the stratosphere. *J. Geophys. Res.* **106**: 7917–7935.

Aref H. 1984. Stirring by chaotic advection. *J. Fluid Mech.* **143**: 1–21.

Bowman KP. 1993. Barotropic simulation of large-scale mixing in the Antarctic polar vortex. *J. Atmos. Sci.* **50**: 2901–2914.

Bowman KP. 1995. Diffusive transport by breaking waves. *J. Atmos. Sci.* **52**: 2417–2427.

Corbosiero KL, Molinari J, Aiyyer A, and Black ML. 2006: The structure and evolution of Hurricane Elena (1985). Part II: Convective asymmetries and evidence for vortex Rossby waves. *Mon. Wea. Rev.* **134**: 3073–3091.

Cram TA, Persing J, Montgomery MT, and Braun SA. 2007: A Lagrangian trajectory view on transport and mixing processes between the eye, eyewall, and environment using a high-resolution simulation of Hurricane Bonnie (1998). *J. Atmos. Sci.* **64**: 1835–1856.

Dritschel DG. 1998. On the persistence of non-axisymmetric vortices in inviscid two-dimensional flows. *J. Fluid. Mech.* **371**: 141–155.

Guinn TA. 1992. A Dynamical Theory for Hurricane Spiral Bands. Ph.D. Dissertation. Colorado State University. 200pp.

Guinn TA, and Schubert WH. 1993. Hurricane spiral bands. *J. Atmos. Sci.* **50**: 3380–3404.

Haynes P, and Shuckburgh E. 2000a. Effective diffusivity as a diagnostic of atmospheric transport, 1. Stratosphere. *J. Geophys. Res.* **105**: 22777–22794.

Haynes P, and Shuckburgh E. 2000b. Effective diffusivity as a diagnostic of atmospheric transport, 2. Troposphere and lower stratosphere. *J. Geophys. Res.* **105**: 22795–22810.

Koh T-Y, and Plumb RA. 2000. Lobe dynamics applied to barotropic Rossby-wave breaking. *Phys. Fluids* **12**: 1518–1528.

Lapeyre G. 2002. Characterization of finite-time Lyapunov exponents and vectors in two-dimensional turbulence. *Chaos* **12**: 688–698.

McIntyre ME, and Palmer TN. 1983. Breaking planetary waves in the stratosphere. *Nature* **305**: 593–600.

McIntyre ME, and Palmer TN. 1984. The 'surf zone' in the stratosphere. *J. Atmos. Terrest. Phys.* **46**: 825–849.

McIntyre ME, and Palmer TN. 1985. A note on the general concept of wave breaking for Rossby and gravity waves. *Pure Appl. Geophys.* **123**: 964–975.

Melander MV, McWilliams JC, and Zabusky MJ. 1987. Axisymmetrization and vorticity gradient intensification of an isolated two-dimensional vortex. *J. Fluid Mech.* **178**: 137–159.

Nakamura N. 1996. Two-dimensional mixing, edge formation, and permeability diagnosed in area coordinates. *J. Atmos. Sci.* **53**: 1524–1537.

Ngan K, and Shepherd TG. 1999a. A closer look at chaotic advection in the stratosphere. Part I: Geometric structure. *J. Atmos. Sci.* **56**: 4134–4152.

Ngan K, and Shepherd TG. 1999b. A closer look at chaotic advection in the stratosphere, Part II: Statistical diagnostics. *J. Atmos. Sci.* **56**: 4153–4166.

Ottino JM. 1989. The kinematics of mixing: stretching, chaos, and transport. Cambridge University Press, 364 pp.

Pierrhumbert RT, and Yang H. 1993. Global chaotic mixing on insentropic surfaces. *J. Atmos. Sci.* **50**: 2462–2480.

Polvani LM, and Plumb RA. 1992. Rossby wave breaking, microbreaking, filamentation, and secondary

vortex formation: the dynamics of a perturbed vortex. *J. Atmos. Sci.* **49**: 462–476.

Reasor PD, Montgomery MT, Marks FD, and Gamache JF. 2000. Low-wavenumber structure and evolution of the hurricane inner core observed by airborne dual-Doppler radar. *Mon. Wea. Rev.* **128**: 1653-1680

Scott RK, Shuckburgh EF, Cammas JP, and Legras, B. 2003. Stretching rates and equivalent length near the tropopause. *J. Geophys. Res.* **108**: 4384, doi:10.1029/2002JD002988.

Shuckburgh E, and Haynes P. 2003. Diagnosing transport and mixing using a tracer-based coordinate system. *Phys. Fluids* **15**: 3342–3357.

Waugh DW, et al. 1994. Transport of material out of the stratospheric Arctic vortex by Rossby wave breaking. *J. Geophys. Res.* **99**: 1071–1088.

Winters KB, and D'Asaro EA. 1996. Diascalar flux and the rate of fluid mixing. *J. Fluid Mech.* **317**: 179–193.